J|A|C|S COMMUNICATIONS

Published on Web 08/19/2009

Controlled Growth of Monodisperse Self-Supported Superparamagnetic Nanostructures of Spherical and Rod-Like $CoFe_2O_4$ Nanocrystals

Ningzhong Bao,* Liming Shen, Yu-Hsiang A. Wang, Jianxing Ma, Dipanjan Mazumdar, and Arunava Gupta*

Center for Materials for Information Technology, University of Alabama, Tuscaloosa, Alabama 35487

Received July 13, 2009; E-mail: nzhbao@mint.ua.edu; agupta@mint.ua.edu

Monodisperse superparamagnetic (SP) nanostructures have drawn significant attention because of their weak magnetic interaction in suspension, high dispersibility in solvents, and large surface area.[1] When the size is below a critical value (typically <10 nm), nanoparticles behave as a single magnetic domain, exhibiting SP behavior above the so-called blocking temperature.[2] The individual nanoparticles possess a magnetic moment but, because of thermal activation, behave like a giant paramagnetic atom. They respond rapidly to an applied magnetic field, while exhibiting negligible remanence and coercivity. These features make SP nanoparticles (nanocrystals) attractive for a broad range of biomedical applications, primarily because agglomeration resulting from strong magnetic interaction is avoided. However, a low magnetization per particle caused by the small size (~10 nm) limits their usage in a number of practical applications since they cannot be effectively separated and controlled by using moderate magnetic fields. Increasing the particle size increases the saturation magnetization, but at the expense of inducing the SP-ferromagnetic transition, and thus the nanoparticles are no longer readily dispersible in solution. Much effort has therefore been focused on the preparation of large-size SP particles using composites.[2] An alternate strategy of forming large complex structures of SP nanocrystals linked by organic chains appears more attractive because of the advantage of increasing the magnetization in a controllable manner while retaining the SP characteristics.[3]

Herein, we report on the shape- and structure-controlled synthesis of self-supported monodisperse cobalt ferrite ($CoFe_2O_4$) SP nanostructures of both spherical and cubic morphology. The individual nanostructures are composed of intergrown spherical or rod-like $CoFe_2O_4$ nanocrystals. We recently reported on a simple thermolysis route for the synthesis of monodisperse ferrite nanocrystals in a high boiling-point solvent utilizing a mixed metal oleate precursor.[4a] By varying the reaction conditions the crystal shape can be readily tuned.[4b] Additional experiments have surprisingly revealed that introduction of boiling bursts by periodic injection of a small amount of hexane during the heating and aging steps can induce self-assembly and secondary growth of the $CoFe_2O_4$ nanocrystals. This results in the formation of larger more complex nanostructures with tunable morphology, size, structure, and magnetic properties.

The shape, size, and structure of the as-synthesized $CoFe_2O_4$ nanostructures have been investigated using transmission electron microscopy (TEM). Figure 1 shows typical TEM images of two different nanostructures obtained by aging at 320 °C for 2 min. By merely changing the heating rate, the product shape and size vary from being spherical (40.5 ± 4.5 nm, Figure 1a−c) to cubic (36.5 ± 2.5 nm, Figure 1d−f). These nanostructures are composed of individual spherical nanocrystals of <5 nm in size (Figure 1c) or nanorods with dimensions of ~3.6 nm in diameter and <25 nm in length (Figure 1f), respectively. They can form highly ordered two-dimensional (2D) assemblies over a large area (SI 1−2).

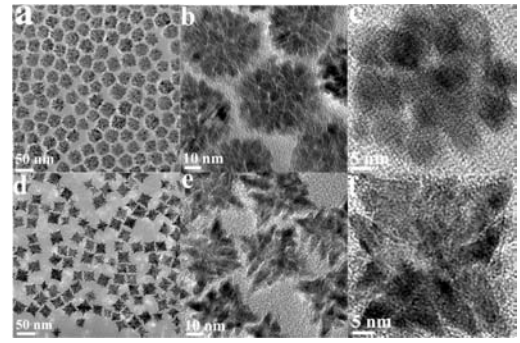

Figure 1. TEM images of monodisperse self-supported (a−c) spherical and (d−f) cubic nanostructures composed of intergrown spherical and rod-like $CoFe_2O_4$ nanocrystals, respectively.

To better understand the formation mechanism, we studied the nucleation, self-assembly, and secondary growth of the $CoFe_2O_4$ nuclei leading to the formation of the nanostructures shown in Figure 1. Without hexane injection, only monodisperse nanocrystals are formed through initial homogeneous nucleation and subsequent diffusion-controlled growth of the initial nuclei.[5] With interval injection of hexane into the reaction mixture during the heating cycle, novel types of complex nanostructures (Figure 1) are produced. This is likely because the burst boiling accompanied by a temperature drop slows down the growth of the nuclei and promotes their assembly to form clusters by particle coalescence (from interaction between the nuclei)[5] or oriented attachment[6] to decrease the surface energy. The uniform nuclei initially formed at 305 °C during synthesis of both types of nanostructures are the same as those formed without hexane injection but are difficult to observe because of the very small size (<2 nm). However, with increasing the temperature to 314 °C, novel monodisperse nanostructures composed of assembled nanocrystals are produced, which is very different from the monodisperse single-crystalline nanocrystals formed in a steady heating process without hexane injection.[4,7]

At 314 °C, spherical nanostructures are formed from assembly of 2D agglomerates of tens of nanocrystals by "particle coalescence" (Figure 2a).[5] On further heating to 320 °C, they grow larger, forming three-dimensional (3D) nanocrystal agglomerates with similar morphology as the final product but are nonuniform in size (Figure 2b). Interestingly, by aging at 320 °C for just 2 min, the uniformity is considerably improved, resulting in monodisperse 3D spherical nanostructures of assembled spherical nanocrystals (Figure 1a−c). By prolonging the aging time, the nanocrystal subunits increase in size and become more densely packed, but the nanostructures' overall shape and size are maintained (SI 3). This is also reflected in the systematic narrowing of the (400) XRD peak with increased aging time (SI 4).

10.1021/ja905811h CCC: $40.75

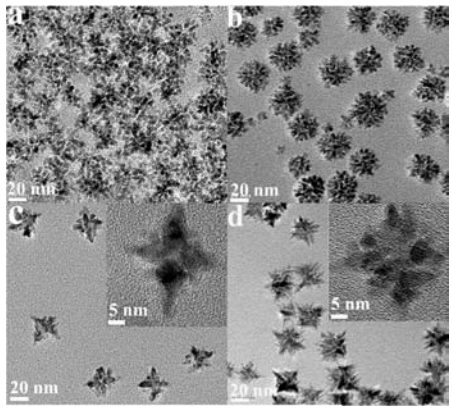

Figure 2. TEM images of intermediate products formed at (a, c) 314 °C and (b, d) 320 °C without aging show the formation of (a, b) spherical and (c, d) cubic self-assembled nanostructures. HRTEM images (the insets) of the dominant nanostructures show the increasing number and length of rod-like subunits resulting in the formation of near-cubic nanostructures.

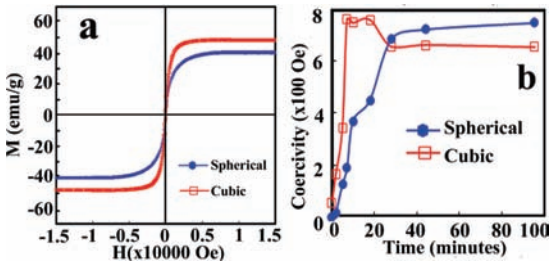

Figure 3. (a) Room-temperature hysteresis loops of spherical and cubic nanostructures after 2 min aging at 320 °C. (b) The change in the coercivity of spherical and cubic nanostructures versus aging time.

The cubic nanostructures are formed when using a lower heating rate (5 °C/min) than that used for the spherical variant (10 °C/min). They evolve from small 3D dendrite-like nanocrystals with a few branches at 314 °C (Figure 2c) to larger and more complex dendridic nanostructures with a full complement of branches at 320 °C (Figure 2d). By aging at 320 °C for 2 min, the mature cubic nanostructures of assembled nanorods are formed (Figure 1d−f), likely resulting from "oriented attachment".[6] By prolonging the aging time, the nanorods tend to convert to more spherical shapes and fuse together to form a more densely packed structure to lower the surface energy (SI 5).

The room-temperature magnetization curves (Figure 3a) display relatively high saturation magnetization values of 40.2 and 49.5 emu/g for the spherical and cubic nanostructures, respectively, after 2 min of aging at 320 °C. These values are, however, somewhat lower than the bulk value (71.2 emu/g). The unique self-supported nanocystal assemblies exhibit SP behavior at room temperature even though the size of an individual assembly exceeds 10 nm. The hysteresis loop shows essentially no coercivity (H_C) for the spherical nanostructures and a low value of 134 Oe for the cubic nanostructures, suggesting that the crystalline subunits are magnetically decoupled. Based on *Langevin* fits[8] to the magnetization loops at 300 K (SI 6), the estimated sizes are 3.9 nm in diameter for the spherical nanostructures and 8.2 nm in length (assuming a 3.6 nm rod diameter) for the cubic nanostructures, respectively. These values match well with the average sizes of the nanocrystal subunits observed by TEM. The thermal energy can overcome the anisotropy energy barrier for these sizes and the net magnetization of the nanocrystal assemblies in the absence of an external field averages to zero. After prolonged aging for 3 h, both the saturation magnetization and the coercivity for the spherical nanostructures at room temperature increase to 50.6 emu/g and 540 Oe, respectively (SI 7). Similarly, the saturation magnetization for the cubic nanostructures increases to 62.3 emu/g, and the coercivity to 1200 Oe (SI 7). Thus, improved coalescence of the crystallites in the nanostructures results in increased magnetic coupling and higher magnetization.

The coercivity is actually tunable by varying the aging time. As seen in Figure 3b, a rapid increase in the H_C is initially observed for both types of nanostructures because of the rapid growth of the nanocrystals during the initial stage. By further increasing the aging time, the spherical nanocrystals grow more slowly, and thereby the H_C of spherical nanostructures essentially maintains a stable value. In contrast, the nanocrystal subunits of the cubic nanostructures experience a simultaneous rodlike-to-spherical shape change and a size increase with longer aging. This is reflected in the somewhat more complex variation in the coercivity, resulting from the combined influence of changes in the shape anisotropy and surface magnetic disorder/pinning.[4c,9]

In summary, we have synthesized highly ordered, self-supported magnetic nanostructures composed of spherical and rod-like colloidal $CoFe_2O_4$ nanocrystals with uniform size. The nanostructures exhibit SP properties at room temperature and respond much more strongly to an external magnetic field than the individual nanocrystals due to their higher moment. The uniform size, complex shapes and structures, and SP properties make these nanostructures attractive for biomedical and other applications. We believe the present synthetic strategy and the results are extendible to the synthesis, shape control, and surface modification of nanocrystals of a variety of other magnetic oxides.

Acknowledgment. This work was supported by NSF under Grant No. ECS-0621850.

Supporting Information Available: Experimental details and Figures SI 1−7. These material are available free of charge via the Internet at http://pubs.acs.org.

References

(1) (a) Mathiowitz, E.; Jacob, J. S.; Jong, Y. S.; Carino, G. P.; Chickering, D. E.; Chaturvedi, P.; Santos, C. A.; Vijayaraghavan, K.; Montgomery, S.; Bassett, M.; Morrell, C. *Nature* **1997**, *386*, 410–414. (b) Schmidt, H. T.; Ostafin, A. E. *Adv. Mater.* **2002**, *14*, 532–535. (c) Sun, Y.; Xia, Y. *Science* **2002**, *298*, 2176–2179. (d) Perez, J. M.; Loughlin, T. O.; Simeone, F. J.; Weissleder, R.; Josephson, L. *J. Am. Chem. Soc.* **2002**, *124*, 2856–2857.
(2) (a) Lu, A. H.; Salabas, E. L.; Schuth, F. *Angew. Chem., Int. Ed.* **2007**, *46*, 1222–1244. (b) Liu, C.; Zou, B.; Rondinone, A. J.; Zhang, Z. J. *J. Am. Chem. Soc.* **2000**, *122*, 6263–6267. (c) Deng, Y.; Qi, D.; Deng, C.; Zhang, X.; Zhao, D. *J. Am. Chem. Soc.* **2008**, *130*, 28–29. (d) Ge, J.; Hu, Y.; Zhang, T.; Yin, Y. *J. Am. Chem. Soc.* **2007**, *129*, 8974–8975.
(3) (a) Ge, J.; Hu, Y.; Yin, Y. *Angew. Chem., Int. Ed.* **2007**, *46*, 1–5. (b) Ge, J.; Hu, Y.; Biasini, M.; Beyermann, W. P.; Yin, Y. *Angew. Chem., Int. Ed.* **2007**, *46*, 4342–4345. (c) Li, X. H.; Zhang, D. H.; Chen, J. S. *J. Am. Chem. Soc.* **2006**, *128*, 8382–8383.
(4) (a) Bao, N.; Shen, L.; Wang, Y.; Padhan, P.; Gupta, A. *J. Am. Chem. Soc.* **2007**, *129*, 12374–12375. (b) Bao, N.; Shen, L.; An, W.; Padhan, P.; Turner, C. H.; Gupta, A. *Chem. Mater.* **2009**, *21*, 3458–33468. (c) Bao, N.; Shen, L.; Padhan, P.; Gupta, A. *Appl. Phys. Lett.* **2008**, *92*, 173101.
(5) (a) Zheng, H.; Smith, R. K.; Jun, Y.; Kisielowski, C.; Dahmen, U.; Alivisatos, A. P. *Science* **2009**, *324*, 1309–1312. (b) Privman, V.; Goia, D. V.; Park, J.; Matijevic, E. *J. Colloid Interface Sci.* **1999**, *213*, 36–45.
(6) (a) Yin, Y.; Alivisatos, A. P. *Nature* **2005**, *437*, 664–670. (b) Penn, R. L.; Banfield, J. F. *Science* **1998**, *281*, 969–971. (c) Narayanaswamy, A.; Xu, H.; Pradhan, N.; Kim, M.; Peng, X. *J. Am. Chem. Soc.* **2006**, *128*, 10310–10319. (d) Penn, R. L.; Banfield, J. F. *Science* **1998**, *281*, 969–971.
(7) (a) Kwon, S. G.; Piao, Y.; Park, J.; Angappane, S.; Jo, Y. N.; Hwang, M.; Park, J. G.; Hyeon, T. *J. Am. Chem. Soc.* **2007**, *129*, 12571–12584. (b) Park, J.; An, K.; Hwang, Y.; Park, J. G.; Noh, H. J.; Kim, J. Y.; Park, J. H.; Hwang, N. M.; Hyeon, T. *Nat. Mater.* **2004**, *3*, 891–895.
(8) Cullity, B. D. *Introduction to Magnetic Materials*; Addison-Wesley: 1972.
(9) (a) Néel, M. L. *J. Phys. Radium* **1954**, *15*, 225–239. (b) Song, Q.; Zhang, Z. J. *J. Am. Chem. Soc.* **2004**, *126*, 6164–6168. (c) Vestal, C. R.; Zhang, Z. J. *J. Am. Chem. Soc.* **2003**, *125*, 9828–9833.

JA905811H